ELSEVIER

Journal of Structural Geology 27 (2005) 317–325

JOURNAL OF STRUCTURAL GEOLOGY

www.elsevier.com/locate/jsg

Geometry, scaling relations and spacing of vertically restricted normal faults

Roger Soliva*, Antonio Benedicto

Dpt. Sciences de la Terre, Orsayterre, FRE2566, Université Paris XI, 91405 Orsay cedex, France

Received 15 September 2003; received in revised form 7 June 2004; accepted 31 August 2004
Available online 26 November 2004

Abstract

The role of the mechanical stratigraphy on fault scaling relations and fault displacement distribution along strike is a subject of recent discussions, poorly documented by field examples. It has, however, a crucial importance in understanding the growth of fault populations where the lithologic alternation shows strong mechanical contrasts. Here, we analyze a population of exceptionally well-exposed and preserved minor normal faults, vertically restricted to a brittle carbonate series by overlying and underlying plastic clay layers. Analysis of fault scarps observed on the same bedding plane reveals that displacement profiles evolve from a linear to a flat-topped distribution once the faults become vertically restricted at the plastic clay layers. This accounts for a transition from a linear to a power-law relationship between displacement and along strike trace length, implying that large vertically restricted faults accommodate less relative strain than unrestricted faults. The analyzed fault population also reveals a nearly regular spacing, with a limiting small distance between large faults, and an exponential fault size distribution. We argue that these fault statistics may be related to a reduction in the stress shadowing development related to the specific shape of the restricted faults. As a consequence, for a given strain, vertically restricted normal fault systems require more large faults than unrestricted systems.

Keywords: Normal faults; Vertical restriction; Displacement profile; Scaling relations; Spacing

1. Introduction

In the last decades, fault maximum displacement–length (D_{max}–L) and size distribution relations have been a topic of much discussion, which has mainly focused on the understanding of the factors controlling the scaling laws (e.g. Walsh and Watterson, 1988; Cowie and Scholz, 1992; Schultz and Fossen, 2002). These relations are fundamental because they allow quantitative analysis of the growth of fault systems (Cowie et al., 1995; Cartwright et al., 1996; Marret et al., 1999; Ackermann et al., 2001), and constitute strong constraints on estimating deformation in the upper crust (e.g. Scholz and Cowie, 1990). These relations also allow the prediction of fault dimensions and fault continuity (Pickering et al., 1997; Maerten et al., 2000; Hardacre and Cowie, 2003) and thus are useful for applications concerning seismic hazard assessment, oil and gas exploration, hydrogeology, and waste storage.

Fault displacement distributions are strongly sensitive to different processes of fault growth such as fault elastic–static interaction (e.g. Bürgmann et al., 1994; Willemse, 1997) allowing asymmetric displacement distributions and an increase in the D_{max}/L ratio (e.g. Gupta and Scholz, 2000a), which can explain a power-law fault size distribution (Cowie et al., 1995; Marret et al., 1999; Hardacre and Cowie, 2003). Recent works propose that fault vertical restriction inherently related to the mechanical stratigraphy (stratigraphic restriction, see Wilkins and Gross (2002) for definition), as observed in cross-sections of layered rocks (e.g. Nicol et al., 1996) or fault systems confined to the elastic thickness of the crust (Jackson and White, 1989; Scholz and Contreras, 1998), results in modifications of the fault scaling relation between D_{max} and fault height (H, or cross-sectional trace length) (Gross et al., 1997; Wilkins and Gross, 2002). A recent theory based on observations from

* Corresponding author. Tel.: +33-169156797; fax: +33-169154911
E-mail address: soliva@geol.u-psud.fr (R. Soliva).

0191-8141/$ - see front matter © 2004 Elsevier Ltd. All rights reserved.
doi:10.1016/j.jsg.2004.08.010

deformation bands (Schultz and Fossen, 2002) proposes a mechanical solution that explicitly relates fault displacement to fault dimensions, both L and H. This analytical solution predicts a decrease of the D_{max}/L ratio if the faults grow only by lengthening, i.e. increasing their aspect ratio (L/H). This D_{max}/L ratio reduction is consistent with the increase of the D_{max}/H ratio occurring at the same time on the vertical dimension, and which can be favored by the contrasting rheology of the mechanical stratigraphy (Bürgmann et al., 1994). Although field observations and modeling clearly show the influence of the mechanical stratigraphy on the fault vertical dimension, there still exists a lack of field data documentation concerning fault displacement distribution along strike.

In this paper, we present an exceptionally clear field example of vertically restricted mesoscale normal faults in marly limestone–silty clays alternation. Measures of fault displacement along strike reveal the scalar dependence of displacement distribution and D_{max}–L scaling with respect to the mechanical stratigraphy. We also discuss the dependence of fault spacing and fault size distribution statistics on the specific shape and the displacement distribution of vertically restricted faults.

2. Geological setting and data acquisition

The faults are well-exposed and preserved on several outcrops in the lignite quarries of the "Collado de Fumanyá" (Carbones de Berga S. A., Catalonia, Spain, 1°47′49″ of longitude and 42°10′54″ of latitude), located in the periclinal closure of the south Pyrenean Serra d'Ensija anticline of the Pedraforca thrusting unit (Vergés and Martinez-Rius, 1988) (Fig. 1a). The faults are observed as a ~4.5-m-thick series of early Maestrichtian marly limestones, dipping 30–70° to the east. Back tilting of bedding to horizontal shows that the studied faults are of normal fault type with an average angle of 60° between conjugate sets, which probably formed during the Pedraforca unit emplacement related to the Pyrenean shortening (Coney et al., 1996).

Bedding planes and cross-section exposures of the marly limestones series reveal that the studied faults terminate against the overlying and underlying silty clay layers, i.e. they are restricted at their top and their base (vertically restricted or confined in the sense of Schultz and Fossen, 2002) (Fig. 1b and c). Exposures of the fault terminations of the restricted faults along dip show that the fault displacements are accommodated by plastic deformation of the silty clay layers, which act as inelastic barriers (or weak barriers in the sense of Manighetti et al. (2001)) (Fig. 1d). This kind of barrier strongly differs from the rigid barriers (or strong barriers) observed by Wilkins and Gross (2002) in layered rocks. Different exposures on the same bedding plane, which is located near the top of the marly limestone series, exhibit a large number of fault scarps indicating normal offsets. More than 500 fault scarps can be observed on the largest studied outcrop (Fig. 1e). Analysis of displacements and distribution of the fault scarps observed on the same bedding plane is the focus of the present work and is detailed in Sections 3 and 4.

Displacement (net slip) of the smaller faults (faults for which the distance comprised between D_{max} and the fault tip $L_d < 4$ m), assessed by offset bedding plane, was measured utilizing millimeter- to meter-scale rulers. Displacement profiles were measured as scarp height versus distance along the scarps. On these faults, measures of normal offset are justified because slickenlines rake steeply. On larger faults ($L_d > 4$ m) displacement profiles were established from photographs of fault scarps revealing clean fresh fault surfaces (Fig. 1f). Photographs were captured with digital-video camera with the optic axis oriented normal to the fault plane. Using laser theodolite and tape measurements, we calibrated the dimensions of the fault scarps and constructed displacement profiles. The major source of error is the amount of fault scarp erosion, estimated at about ± 1 cm on average. Fault lengths and spacing of the fault population observed on the same bedding plane were measured on a scale-calibrated interpretation of a detailed photo-mosaic of the outcrop shown in Fig. 1e. Fault spacing was recorded on the photo-mosaic interpretation along a 165-m-long scan line oriented perpendicular to the average fault strike.

Some of the large normal faults described in this paper show overprinted oblique and strike-slip slickenlines indicating fault reactivation subsequent to normal faulting. When this occurs, the fault ends can only show oblique striations that are interpreted as the result of the propagation of the fault tip during the reactivation stage. The dimension of these fault ends are relatively small (in the best case ~1.5 m on larger faults having $L \sim 40$ m) suggesting that the amount of normal displacement due to oblique or strike-slip reactivation, if any, is negligible. Some calcite filled pull-apart structures associated with oblique slickenlines indicate a normal component of displacement due to reactivation lower than 10% of the scarp height. Reactivated faults will be distinguished by different symbols on graphs.

3. Displacement distribution and D_{max}–L relations

Only displacement profiles along the distance comprised between D_{max} and the fault tip (L_d) of simple "isolated half faults" have been studied. An isolated half fault is defined as the fault part comprised between D_{max} and a fault tip which is not linked and non-interacting with another surrounding fault tip (see also Gupta and Scholz, 2000a,b), i.e. with no branching or relay ramping able to transfer the displacement to another fault (e.g. Peacock and Sanderson, 1991; Soliva and Benendicto, 2004) (see, for example, the isolated fault of Fig. 1f). The studied isolated half faults observed on the largest outcrop are labeled on Fig. 1e.

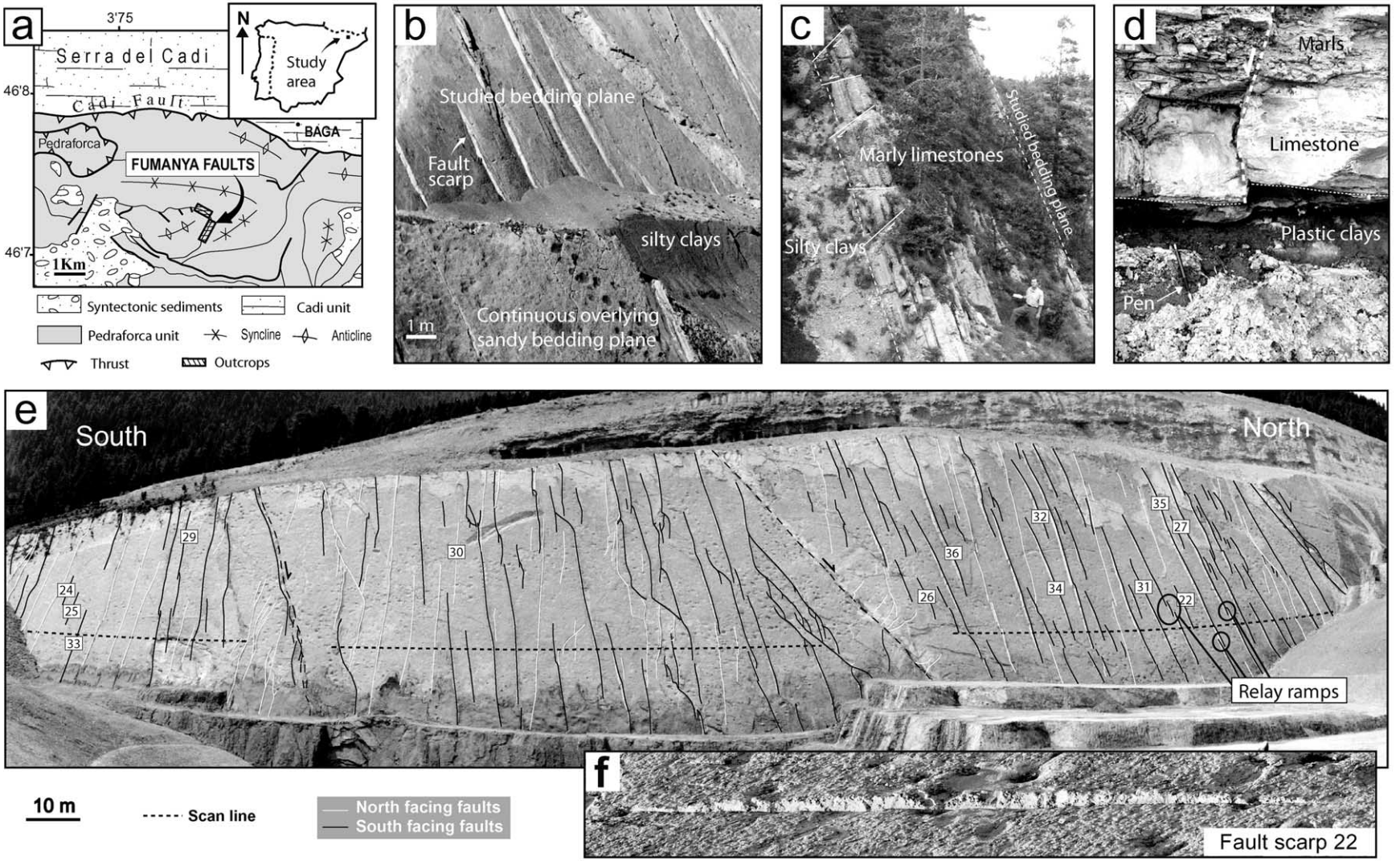

Fig. 1. Overview of the Fumanyá fault system. (a) Location of the study area in the South Pyrenees. (b) Bedding planes exposure of the top of the studied marly limestone series showing that the faults terminate in the overlying silty clay layer. (c) Cross-sectional exposure of the studied faults showing that the faults also terminate in the underlying silty clay layer. (d) Photograph of a detailed exposure of a fault termination in the underlying silty clays of plastic behavior. (e) Photograph of the largest studied outcrop showing the high dipping bedding plane of marly limestones displaced by hundreds of faults. The studied conjugate fault scarps are shown as black and white lines, i.e. south and north facing, respectively. Thin broken lines are strike-slip faults kinematically coherent with the studied tilted normal faults. The thick broken line is the position of the scan line along which fault spacing has been measured on a better-defined photo-mosaic after scalar calibration. Numbers labeled on the photograph show the studied isolated half faults (see the main text for definition) of Figs. 2 and 3 observed on this outcrop. (f) Example of a normal fault scarp of an isolated fault.

Normalized displacement profiles of isolated half faults (Fig. 2a) exhibit clear differences in profile shape as a function of fault length. Ten displacement profiles of different size, selected from Fig. 2a, are shown in Fig. 2b. Small faults (gray profiles) exhibit a nearly linear displacement decrease from D_{max} toward the fault tips (peaked profile shape), with a mean displacement gradient of 0.073. The profiles of large faults are generally flat-topped, which is best expressed by the largest faults. These profiles can be divided into two near linear parts of different slope separated by a smooth deflection point. The part comprised between D_{max} and the deflection point (up to ~70% of L on the largest faults) is flat with a very low, nearly constant displacement gradient ranging between 0.004 and 0.017. In contrast, the part between the deflection point and the fault tip shows a higher gradient, ranging between 0.044 and 0.074, comparable with that of the small faults.

Flat-topped fault displacement distribution along strike is well documented from field data (Dawers et al., 1993; Fossen and Hesthammer, 1997; Manighetti et al., 2001) and is consistent with stratigraphic restriction when it appears as a function of fault length. On the basis that fault dimensions control the amount of displacement ($D_{max} = \gamma L^n$, where n is the exponent and γ is a constant; see Cowie and Scholz, 1992; Schlische et al., 1996; Schultz and Fossen, 2002), we infer that zones having low gradients (nearly constant displacement along strike) reflect the restricted part of large faults because they must have a nearly constant height along their central parts (Fig. 2c). A critical height ($H_c = T/\sin\alpha$), defined as the height of the vertically restricted faults, given by the brittle layer thickness (in our study $T \sim 4.5$ m) and fault dip ($\alpha \sim 60°$), likely controls the amount of displacement. In contrast, the steeper displacement gradient bounding this central section must represent the parts of the fault that are not vertically restricted. Fault half-length (L_d) is ~4 m when the faults become flat-topped (Fig. 2a and b), and H_c must be ~5 m. Hence, we estimate the fault aspect ratio (L/H_c) at the initiation of restriction to be ~2, because as we only observe the upper part of the faults, L is probably underestimated.

Fig. 3a and b shows D_{max}–L_d data of the faults presented in Fig. 2a, with six added small faults ($L_d < 4$ m) for which the entire profiles were not measured because of the large amount of erosion or the difficulty in reading the displacement near the fault end. The data show, on both bi-log and linear axes representations, that two different scaling relations can be used to describe the fault population (equations are labeled on the graph). A small fault

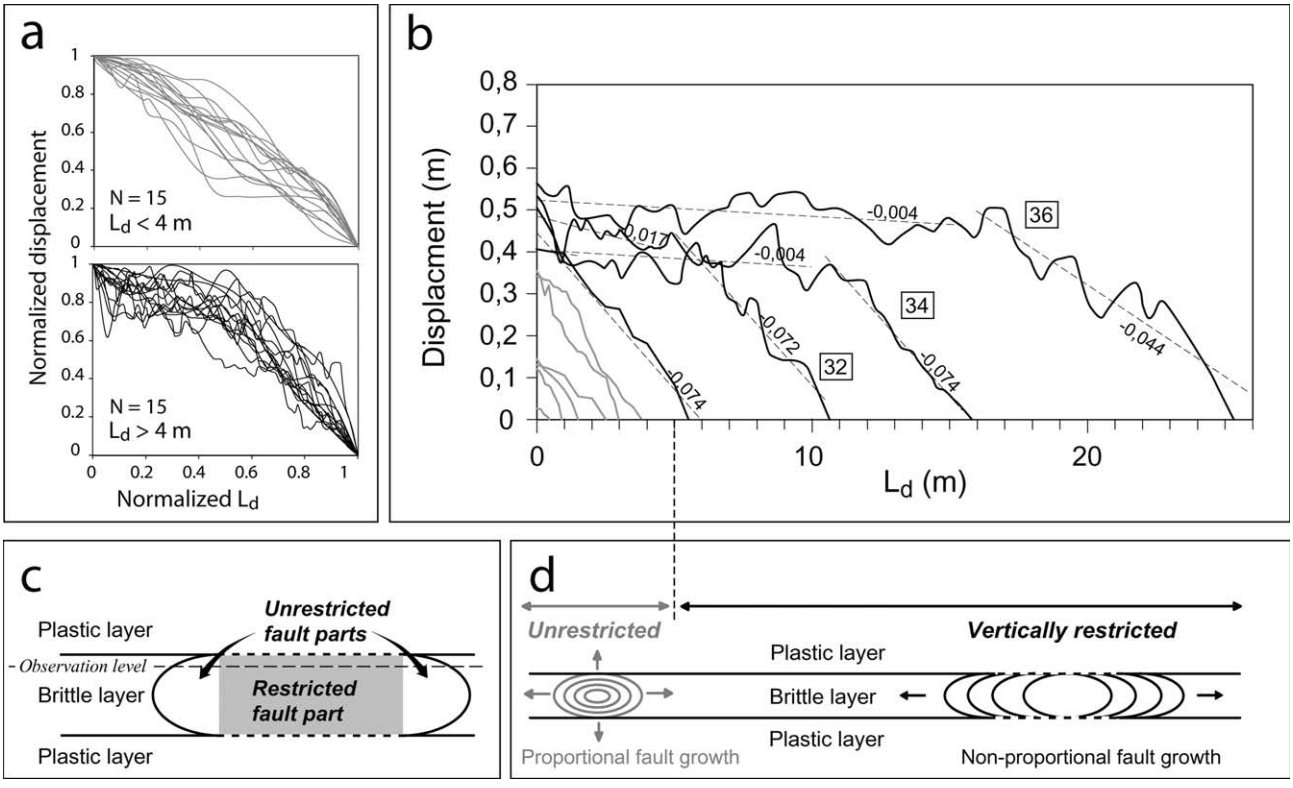

Fig. 2. (a) Thirty normalized displacement profiles comprised along L_d the distance between D_{max} and fault tip. Profiles are sorted into two groups, small faults ($L_d < 4$ m) and large faults ($L_d > 4$ m). N is the number of presented profiles. (b) Ten selected half-profiles of different sizes ($0.4 < L_d < 25.3$ m). Gray and black profiles are small and large faults, respectively. Thin broken lines are best linear fits of portions of displacement profiles, with gradients labeled. Numbers labeled near the profiles of large faults refers to Fig. 1e. (c) Illustration of an entire fault plane vertically restricted within a brittle layer having restricted and unrestricted fault parts. (d) Interpretation of fault displacement profiles in 3-D proportional and non-proportional fault growth within a brittle layer.

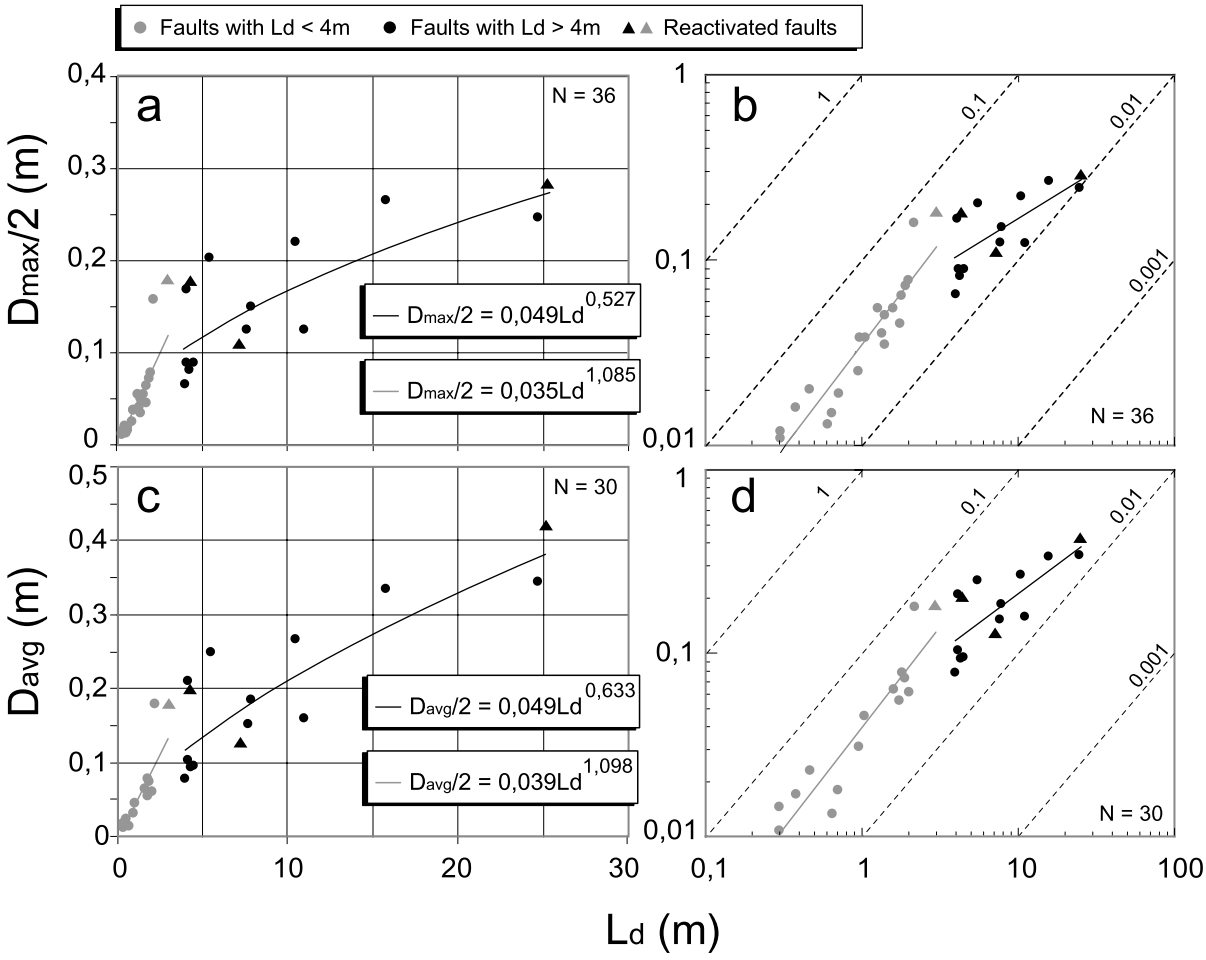

Fig. 3. Representations of the displacement–length data of the studied fault population. (a) and (b) Linear and bi-log plots, respectively, of $D_{max}/2$ vs. L_d for small ($L_d \leq 4$ m, gray dots) and large ($L_d > 4$ m, black dots) isolated faults (see text for definition). (c) and (d) Linear and bi-log plots, respectively, of D_{avg} vs. L_d of the same data for which displacement profiles have been established (Fig. 2a) (see text for further explanation and definition of D_{avg}). Triangular symbols are used for reactivated faults. Gray and black lines are best linear fit for small faults and power-law fit for large faults, respectively, with equation labeled. Also shown are lines of constant $(D_{max}/2)/L_d$ (broken lines) with values labeled.

population, non-restricted and characterized by peaked profile shape, can be explained by a nearly linear relation between D_{max} and L_d ($D_{max} = \gamma L_d^n$, with $n = 1.085$ close to 1, $\gamma = 0.035$ and least square coefficient $R^2 = 0.867$), which is consistent with a cohesive end-zone model of faulting in 2-D (Cowie and Scholz, 1992) or 3-D (Schultz and Fossen, 2002). The data of the large fault population are scattered, a best linear fit ($D_{max} = \gamma L_d^n$, with $n = 1$ and $\gamma = 0.035$) cannot be used to explain this population (determination coefficient $R^2 = 0.219$). However, this dataset is better explained by a power-law fit ($D_{max} = \gamma L_d^n$, with $n = 0.527$, $\gamma = 0.0497$ and $R^2 = 0.54$).

Because D_{max} could be an outlier value of displacement due to the irregular shapes of the profiles, we have estimated the average displacement (D_{avg}) (see Dawers et al., 1993) on the faults presented in Fig. 2a, for which the profile has been measured. To estimate D_{avg}, we have firstly calculated the surface areas of the scarps using numerical pixel counts of the areas underneath each displacement profile. Then, we have divided the surface area of the scarp by L_d to obtain the estimation of D_{avg}. The graphs of D_{avg}–L_d are presented in Fig. 3c and d. Although less expressed than on D_{max}–L_d graphs, the deflection of the data is still clearly present on both linear and bi-log representations. The reason for the difference between D_{max}–L_d and D_{avg}–L_d graphs, which is discussed in Section 5, is mainly related to the difference in the characteristic shape between small and large faults (Fig. 2a). Hence, a simple and reasonable interpretation of these data is that the D_{max}–L_d relation changes from linear to power-law once the faults become vertically restricted. The observed displacement profiles suggest that in 3-D, the growth of an ideal isolated fault at Fumanyá was proportional between height and length ($L \sim 2H$) before vertical restriction and non-proportional ($L > 2H_c$) after the initiation of the vertical restriction (Fig. 2d). It is also probable that several of the small faults were half-restricted

(only restricted at the top of the marly limestone series), which could explain a component of scatter in this dataset. However, this cannot be clearly inferred from their displacement distribution that generally shows peak shaped profiles.

4. Fault spacing and size distribution

Statistics of fault spacing, measured on the scale calibrated scan line shown in Fig. 1e, are presented in Fig. 4a. Fault spacing was therefore measured in graben and horst fault configurations, and between faults having the same dip direction (see illustration in Fig. 4a). Spacing of the entire fault population exhibits log-normal distribution (also observed in joint sets by Narr and Suppe (1991) and Rives et al. (1992)) with a mode (maximum frequency) for spacing ranging between 2 and 3 m, revealing a nearly regular spacing between large faults. Faults having the same dip direction show a bimodal distribution with the maximum frequency corresponding to the mode of the log-normal distribution. Although very small faults under the photograph resolution or those that are not crosscut by the scan line are ignored, this graph mainly reveals a limiting small distance (1 m) within which no large faults are detected. This smallest spacing between large faults is also qualitatively visible on the photograph of Fig. 1e), on which their spacing appears nearly regular and small compared with their length.

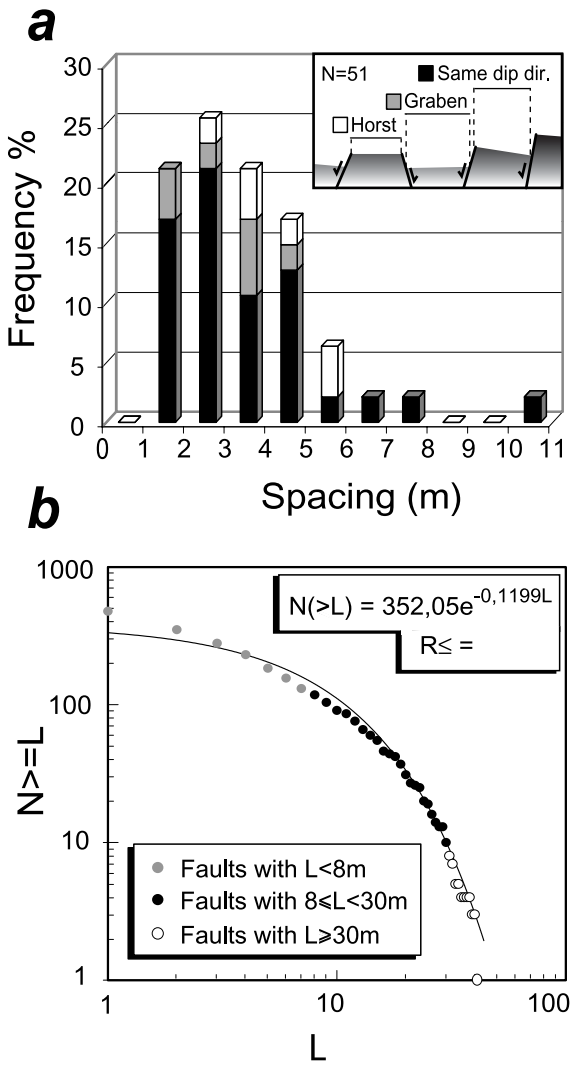

Fig. 4. Fault population statistics. (a) Histogram showing the spacing distribution along the scan line, 165 m long, crossing 51 faults. Faults having the same sense of dip, horst and graben configuration are distinguished. (b) Log plot graph of cumulative fault length frequency. N is defined as the number of faults. Thin line is best-fit exponential, calculated with only faults of $L \leq 30$ m (see the text for explanation), with equation and determination coefficient (R^2) labeled.

It is important to note that the studied faults did not originate as joints, which could have explained the nearly regular spacing observed between faults of the same dip direction. Fault spacing has been related to the stress drop distributions (or shadowing) surrounding the fault within which fault initiation or propagation are impeded (Ackermann and Schlische, 1997; Willemse, 1997; Gupta and Scholz, 2000a,b; Cowie and Roberts, 2001). Stress shadow geometry around a fault is in turn closely related to the 3-D geometry of the faults (aspect ratio) and especially its displacement distribution (Willemse, 1997; Gupta and Scholz, 2000a). We propose that both high aspect ratio and the related flat-topped profiles of the observed large faults lead to a narrow stress shadow close to the faults, and can account for the small and nearly regular spacing between large faults having the same dip direction.

Fig. 4b shows the cumulative fault length frequency distribution of 567 measured faults, including isolated, interacting and hard-linked faults detected on the outcrop of Fig. 1e. The total length of hard-linked faults is considered as that of one fault. Best-fit functions have been calculated first with all the presented dataset ($1 < L < 40$ m); the obtained best-fit function is exponential negative (not presented here). However, because the largest faults are censored (extending beyond the study area), best-fit functions have been secondly calculated with only faults of $L < 30$ m. The exceptionally good exposure of the faults and high-resolution imaging of the scale calibrated photomosaic suggest a truncation bias due to the photo resolution only for faults having $L < 1$ m. With faults of $1 < L < 30$ m, we find that an exponential negative function (equation in Fig. 4b) better explains the data than a power law fit (linear on log plot), which is typically obtained from field examples of non-restricted faults (e.g. Walsh et al., 1991; Marret et al., 1999).

Gupta and Scholz (2000b) for the Afar depression, Spyropoulos et al. (1999) and Ackermann et al. (2001) with monolayer clay models have also observed exponential distributions, which are interpreted to be consistent with regular spacing in a restricted fault system. Numerical

models of a non-restricted fault system (Cowie et al., 1995; Cladouhos and Marret, 1996; Hardacre and Cowie, 2003) have shown that fault coalescence and subsequent stress shadowing dominates over fault nucleation and leads to a power-law distribution. In our case, stress shadow geometry has probably grown non-linearly with fault length because of the fault vertical restriction. As Ackermann et al. (2001) suggested from their modeling, we suggest that the decreased displacement gradient associated with fault restriction results in a relatively reduced stress shadow and thus allows large faults to grow closer to each other. This is a possible reason to account for the large proportion of intermediate and large fault lengths observed in the exponential distribution. In addition, we have found that displacement distribution on restricted faults is flat-topped with a limiting amount of displacement, which implies that large faults accommodate relatively low strain (poorly efficient fault) compared with non-restricted faults. This suggests that for a given strain, restricted fault systems require more large faults than unrestricted systems.

5. Discussion and conclusion

The present paper documents a field example of faults vertically restricted into marly limestone series where the stratigraphic fault restriction occurs due to overlying and underlying plastic silty clay layers. Measurements of fault displacement along strike on the same bedding plane reveal a D_{max}–L relation transition from linear to power-law, inherently related to the evolution of displacement profile from linear to flat-topped distribution. We interpret this transition as the expression of the stratigraphic restriction of the 3-D fault shape.

A break of scaling is also clearly observed with the average value of displacement (D_{avg}–L graphs of Fig. 3c and d). However, on D_{avg}–L graphs the data of the large faults are shifted upward, leading to a smoother deflection of the entire population (compare Fig. 3b and d). Fig. 5 reveals the existence of a discrepancy in the D_{max}/D_{avg} ratio between small (peak shaped profiles) and large (flat-topped profiles) faults. A more scattered D_{max}–D_{avg} data (randomly) and similar D_{max}/D_{avg} average ratio should be expected if D_{max} is an outlier parameter related to displacement irregularity. Indeed, this discrepancy obviously reflects the dependence of D_{avg} in displacement profile shape (peaked or flat-topped shapes), and suggests that this parameter should be carefully used when comparing characteristic fault displacement distribution. The large scattering of the data, especially for the large faults, is therefore probably due to a fault complexity "out of the plane of inspection" as, for example, the presence of an intra marly limestone mechanical barrier, vertical fault segmentation, or local rheological heterogeneity.

Although faulting generally differs from cataclastic frictional sliding and compactional displacement occurring

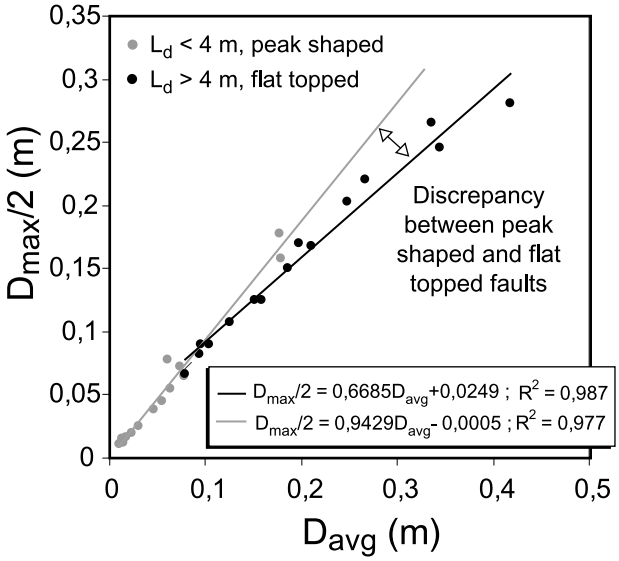

Fig. 5. Graph of D_{max} vs. D_{avg} of the studied fault population. Small (peak shaped profiles) and large faults (flat-topped profiles) are distinguished by different symbols. Best fit equations are labeled with least square coefficients.

in porous sandstones (e.g. Antonellini et al., 1994), similar power-law scaling was observed on deformation bands growing confined to a sandstone layer (Schultz and Fossen, 2002). Both the isolated faults presented in this paper and the isolated deformation bands from Schultz and Fossen (2002) are reported in Fig. 6. The observed power-law scaling of the deformation bands has been explicitly related to fracture development that increases in aspect ratio, i.e. lengthening deformation bands. Regardless of the transition of scaling observed in our dataset, all the faults of the

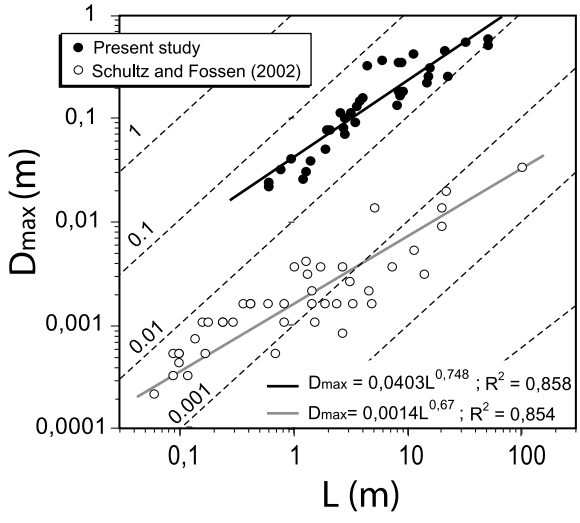

Fig. 6. Bi-log representation of D_{max} vs. L of vertically restricted isolated faults from this study and isolated deformation bands from Schultz and Fossen (2002). For the Fumanyá fault set L corresponds to $2L_d$. Power law fits of each fault population are shown with equations and least square coefficients labeled.

present study can be explained by a similar power law with exponent $n<0$ (see equations in Fig. 6). The similarity of scaling behavior on these different deformation processes leads to the thought that stratigraphic restriction should be efficient in a wide variety of rocks where the lithological alternation shows strong mechanical contrasts. Together with observations of fault geometry in stratigraphic sequences (Nicol et al., 1996; Gross et al., 1997; Schultz and Fossen, 2002; Wilkins and Gross, 2002) this suggests that normal fault vertical restriction is an important process of faulting in the sedimentary cover. For example, it plays an important role in normal fault vertical segmentation (Koledoye et al., 2000; Wilkins and Gross, 2002) and probably also in the 3-D pattern (Benedicto et al., 2003).

Fault vertical restriction is suggested as being a possible process occurring for faulting at a crustal-scale where the ductile crust of inelastic behavior can mechanically inhibit brittle faulting (e.g. Jackson and White, 1989; Scholz and Contreras, 1998). Therefore, displacement distribution along strike, fault size distribution and spacing should be useful for discussing the 3-D fault geometry at a crustal-scale, and the implication for fluid migrations and localization of seismicity. Large normal faults ($L>30$ km) having flat-topped displacement profiles with smooth deflection zones could be regarded as faults restricted at the base of the upper crust. However, on these large faults, other questions are raised concerning the role of ductile shearing in the lower crust, sediment loading or mechanisms like isostatic adjustment that probably affect the displacement distribution.

Acknowledgements

We thank Richard Schultz for fruitful discussions in the field and helpful comments on the manuscript. Thorough reviews by Patience Cowie and Scott Wilkins improved the manuscript. We are grateful to the Carbones de Berga Company, and especially Joan Llobet for permitting access to the quarry, climbing on the outcrops and field assistance.

References

Ackermann, R.V., Schlische, R.W., 1997. Anticlustering of small normal faults around larger faults. Geology 25, 1127–1130.

Ackermann, R.V., Schlische, R.W., Withjack, M.O., 2001. The geometric and statistical evolution of normal fault systems: an experimental study of the effects of mechanical layer thickness on scaling laws. Journal of Structural Geology 23, 1803–1819.

Antonellini, A., Aydin, A., Pollard, P., 1994. Microstructure of deformation bands in porous sandstones at Arches National Park, Utah. Journal of Structural Geology 16, 941–959.

Benedicto, A., Schultz, R.A., Soliva, R., 2003. Layer thickness and the shape of faults. Geophysical Research Letters 30, 2076.

Bürgmann, R., Pollard, D.D., Martel, S.J., 1994. Slip distributions on faults: effects of stress gradients, inelastic deformation, heterogeneous host-rock stiffness, and fault interaction. Journal of Structural Geology 16, 1675–1690.

Cartwright, J.A., Mansfield, C., Trudgill, B., 1996. The growth of normal fault by segment linkage, in: Buchanan, P.G., Nieuwland, D.A. (Eds.), Modern Developments in Structural Interpretation, Validation and Modelling Geological Society Special Publication, 99, pp. 163–177.

Cladouhos, T.T., Marret, R., 1996. Are fault growth and linkage models consistent with power-law distributions of fault lengths? Journal of Structural Geology 18, 281–293.

Coney, P.J., Muñoz, A.J., McClay, K.R., Evenchick, C.A., 1996. Syntectonic burial and post-tectonic exhumation of the southern Pyrenees foreland fold-thrust. Journal of Geological Society of London 153, 9–16.

Cowie, P., Roberts, G.P., 2001. Constraining slip rates and spacing for active normal faults. Journal of Structural Geology 23, 1901–1915.

Cowie, P., Scholz, C.H., 1992. Physical explanation for the displacement–length relationship of fault using a post-yield fracture mechanics model. Journal of Structural Geology 14, 1133–1148.

Cowie, P.A., Sornette, D., Vanneste, C., 1995. Multifractal scaling properties of a growing fault population. Geophysical Journal International 122, 457–469.

Dawers, N.H., Anders, M.H., Scholz, C.H., 1993. Growth of normal faults: displacement–length scaling. Geology 21, 1107–1110.

Fossen, H., Hesthammer, J., 1997. Geometric analysis and scaling relations of deformation bands in porous sandstones. Journal of Structural Geology 19, 1479–1493.

Gross, M.R., Gutiérrez-Alonso, G., Bai, T., Wacker, M.A., Collinsworth, K.B., Behl, R.J., 1997. Influence of mechanical stratigraphy and kinematics on fault scaling relations. Journal of Structural Geology 19, 171–183.

Gupta, A., Scholz, C.H., 2000a. A model of normal fault interaction based on observation and theory. Journal of Structural Geology 22, 865–879.

Gupta, A., Scholz, C.H., 2000b. Brittle strain regime transition in the afar depression: implication for fault growth and seafloor spreading. Geology 28, 1087–1090.

Hardacre, K.M., Cowie, P.A., 2003. Variability in fault size scaling due to rock strength heterogeneity: a finite element investigation. Journal of Structural Geology 25, 1735–1750.

Jackson, J.A., White, N.J., 1989. Normal faulting in the upper continental crust: observations from regions of active extension. Journal of Structural Geology 11, 15–36.

Koledoye, B., Aydin, A., May, E., 2000. Three-dimensional visualization of normal fault segmentation and its implication for fault growth. The Leading Edge 2000; 692–701.

Maerten, L., Pollard, D.D., Karpuz, R., 2000. How to constrain 3-D fault continuity and linkage using reflection seismic data: a geomechanical approach. American Association of Petroleum Geologist Bulletin 84, 1311–1324.

Manighetti, I., King, G.C.P., Gaudemer, Y., Scholz, C.H., Doubre, C., 2001. Slip accumulation and lateral propagation of active normal faults in Afar. Journal of Geophysical Research 106, 13667–13696.

Marret, R., Ortega, O.J., Kelsey, C.M., 1999. Extent of power-law scaling for natural fractures in rock. Geology 27, 799–802.

Narr, W., Suppe, J., 1991. Joint spacing in sedimentary rocks. Journal of Structural Geology 13, 1037–1048.

Nicol, A., Watterson, J., Walsh, J.J., Childs, C., 1996. The shapes, major axis orientations and displacement patterns of fault surfaces. Journal of Structural Geology 18, 235–248.

Peacock, D.C.P., Sanderson, D.J., 1991. Displacement, segment linkage and relay ramps in normal fault zones. Journal of Structural Geology 13, 721–733.

Pickering, G., Peacock, D.C.P., Sanderson, D.J., Bull, J.M., 1997. Modeling tip zones to predict the throw and length characteristics of faults. American Association of Petroleum Geologist Bulletin 81, 82–99.

Rives, T., Razack, M., Petit, J.-P., Rawnsley, K.D., 1992. Joint spacing: analogue and numerical simulations. Journal of Structural Geology 14, 925–937.

Schlische, R.W., Young, S.S., Ackermann, R.V., Gupta, A., 1996. Geometry and scaling relations of a population of very small rift-related normal faults. Geology 24, 683–686.

Scholz, C.H., Contreras, J.C., 1998. Mechanics of continental rift architecture. Geology 26, 967–970.

Scholz, C.H., Cowie, P.A., 1990. Determination of total strain from faulting using slip measurements. Nature 346, 837–839.

Schultz, R.A., Fossen, H., 2002. Displacement–length scaling in three dimensions: the importance of aspect ratio and application to deformation bands. Journal of Structural Geology 24, 1389–1411.

Soliva, R., Benedicto, A., 2004. A linkage criterion for segmented normal faults. Journal of Structual Geology 12, 2251–2267.

Spyropoulos, C., Griffith, W.J., Scholz, C.H., Shaw, B.E., 1999. Experimental evidence for different strain regimes of crack populations in a clay model. Geophysical Research Letters 26, 1081–1084.

Vergés, J., Martinez-Rius, A., 1988. Corte compensado del Pireneo oriental: geometria de las cuencas de ante-paisy edades de empezamiento de los mantos de corrimiento. Acta Geologica Hispanica 23, 95–106.

Walsh, J.J., Watterson, J., 1988. Analysis of the relationship between displacements and dimension of faults. Journal of Structural Geology 103, 239–247.

Walsh, J.J., Watterson, J., Yielding, G., 1991. The importance of small-scale faulting in regional extension. Nature 351, 391–393.

Wilkins, S.J., Gross, M.R., 2002. Normal fault growth in layered rocks at split mountain, Utah: influence of mechanical stratigraphy on dip linkage, fault restriction and fault scaling. Journal of Structural Geology 24, 1413–1429.

Willemse, E.J.M., 1997. Segmented normal faults: correspondence between three-dimensional mechanical models and field data. Journal of Geophysical Research 102, 675–692.